Asymmetrical Load Modulated Balanced Amplifier With Continuum of Modulation Ratio and Dual-Octave Bandwidth

Yuchen Cao, *Graduate Student Member, IEEE*, Haifeng Lyu, *Graduate Student Member, IEEE*, and Kenle Chen, *Member, IEEE*

***Abstract*— This article presents a new load-modulation power amplifier (PA) architecture—asymmetrical load-modulated balanced amplifier (ALMBA). It is for the first time discovered that the control amplifier (CA) of LMBA can be designed with arbitrary load modulation (LM) ratio by offsetting the symmetry of two sub-amplifiers (BA1 and BA2) in the balanced topology. The rigorous analytical derivation reveals a unification of the quadrature-coupler-based LM PA theory, which inclusively covers the recently reported LMBA within this generalized framework. Through pseudo-Doherty (PD) biasing of the asymmetric BA1 & BA2 (peaking) and the CA (carrier) combined with proper amplitude and phase controls, the optimal LM behaviors of three amplifiers can be achieved independently overextended power back-off range and ultrawide RF bandwidth. Importantly, the LM of CA effectively mitigates the over-driving issue imposed on symmetrical PD-LMBA, leading to enhanced overall reliability and linearity. Based on the proposed theory, an RF-input PD-ALMBA is designed and implemented using commercial GaN transistors. The developed prototype experimentally demonstrates dual-octave bandwidth from 0.55 to 2.2 GHz, which is the widest bandwidth ever reported for load-modulation PAs. The measurement exhibits an efficiency of 49–82% for peak output power and 40–64% for 10-dB OBO within the design bandwidth. When stimulated by a 20-MHz long-term evolution (LTE) signal with 10.5-dB peak to average power ratio (PAPR), an average efficiency of 47–63% is measured over the entire bandwidth at an average output power around 33 dBm.**

***Index Terms*— Asymmetrical, balanced amplifier (BA), Doherty, fifth generation (5G), GaN, high efficiency, load modulation (LM), power amplifier (PA), wideband.**

I. Introduction

THE formation of the fifth-generation (5G) wireless communication ecosystem have resulted in ever-growing demands for higher data rates. Due to the scarcity of spectrum resources, low-latency and high-capacity wireless connectivity requires vast enhancement of spectral efficiency realized using advanced modulation schemes, such as 1024 quadrature amplitude modulation (QAM) and orthogonal frequency division multiplexing (OFDM). However, those complexly modulated radio waves have a high peak-to-average power ratio (PAPR), leading to substantially reduced efficiency of traditional power amplifiers (PAs). On the other hand, the proliferation of communication bands has been largely expanding the wireless spectrum toward higher frequencies. This ever-increasing number of allocated frequency bands is strongly calling for bandwidth extension technologies of PAs. In the current and next-generation radio systems, the operational bandwidth of a single PA is desired to be as wide as possible, to minimize the number of PAs on a wireless platform for reducing the cost, space, and system complexity. These emerging requirements have brought up unprecedented challenges for the realization of PAs.

To improve the PA efficiency for amplification of high-PAPR signals, there are currently two main technical solutions, envelope tracking (ET) and load modulation (LM). Due to the fact that ET suffers from the complexity of system implementation, limited dynamic range, and undesirable modulation-bandwidth up-scalability [1], [2], LM technique exhibits promising potential for accommodating the fast-evolving communication standards, for example 5G and Wi-Fi 6. Until now, a variety of LM architectures have been proposed, developed, and implemented in practical systems, including Doherty PA (DPA) [3]–[5], out-phasing PA [6]–[9], and varactor-based dynamic LM [10]–[14]. Among various LM techniques, DPA has already been widely deployed in cellular base stations as a representative implementation of LM [15], [16]. However, toward the applications in the emerging wireless systems, DPA faces two major challenges as follows. First, the limited output power back-off (OBO) range is not sufficient to support the large PAPR of the latest modulation schemes (>10 dB); Second, the RF bandwidth is strongly limited by the quarter-wave inverter embedded in the DPA circuitry. Despite recent advances in broadband DPAs [17]–[20], maintaining consistently optimal load-modulation behavior and efficient DPA performance over a wide RF bandwidth still remains a major challenge.

The recently reported load modulated balanced amplifier (BA) (LMBA) [21]–[26] has been demonstrated as an effective method to perform LM over a wide RF bandwidth. The

Manuscript received May 1, 2020; revised June 18, 2020; accepted June 28, 2020. Date of publication August 31, 2020; date of current version January 5, 2021. This work was supported by the National Science Foundation (NSF) under Award 1914875. This article is an expanded version from the IEEE MTT-S International Microwave Symposium, Los Angeles, CA, USA, June 21–26, 2020. *(Corresponding author: Kenle Chen.)*

The authors are with the Department of Electrical and Computer Engineering, University of Central Florida, Orlando, FL 32816 USA (e-mail: yuchencao@knights.ucf.edu; haifeng@knights.ucf.edu; kenle.chen@ucf.edu).

Color versions of one or more of the figures in this article are available online at https://ieeexplore.ieee.org.

Digital Object Identifier 10.1109/TMTT.2020.3014616

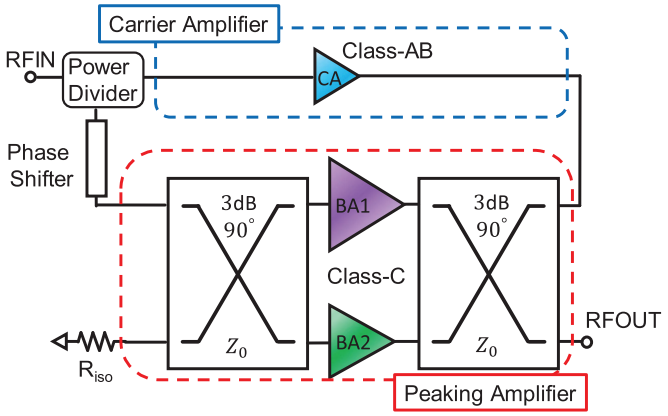

Fig. 1. Overview of PD asymmetrical LMBA.

load impedance of the BA device can be controlled by the amplitude and phase variations of a control signal injected into the isolated port of the output quadrature coupler, leading to enhanced back-off efficiency. By implementing an external control amplifier (CA) to drive the isolation port, an RF-input LMBA can be constructed [22], [27]. The authors of this article has further developed the generic LMBA theory in a new topology [28], [29], which is named pseudo-Doherty (PD) LMBA (PD-LMBA). It reveals that the Doherty-like biasing of BA (peaking) and CA (carrier) combined with proper amplitude and phase controls can result in optimal BA LM behavior overextended OBO range. Moreover, such an operation can be seamlessly extended over an unlimited frequency span as long as proper BA-CA phase offset is maintained. This type of Doherty-like biasing of LMBA has also been reported as sequential LMBA (SLMBA) in [30]. However, there are also some unresolved issues with PD-LMBA. Primarily, the CA reaches saturation at the predetermined OBO level where the BA starts to turn on, but the CA impedance remains constant as the input power continues to increase. This indicates that the CA is constantly subject to over-driving during the BA LM, which could cause strong non-linearity and reliability issues of CA.

Expanding the horizon of LMBA, this article presents a new theory of asymmetrical load-modulated BA (ALMBA). It is discovered that, by setting asymmetric current/power scaling of BA1 and BA2, a continuum of CA load-modulation ratio can be achieved, that is between carrier LM of DPA and no LM of CA in generic LMBA. Meanwhile, the LM behaviors of BA1 and BA2 in PD-ALMBA can be controlled independently. As a result, in PD operation of ALMBA as shown in Fig. 1, the current and power of CA can further increase after reaching the first efficiency peak at the target OBO level, which strongly mitigates the CA over-driving as in PD-LMBA [28]–[30], leading to the enhanced linearity and reliability of the entire amplifier. It is critical to note that the established ALMBA theory inclusively explains the generic symmetrical LMBA mode, which can be considered as a special case of this generalized theoretical framework for quadrature-coupler-based active LM architectures. The analytical derivation of the proposed theory is well verified by simulation and is experimentally validated

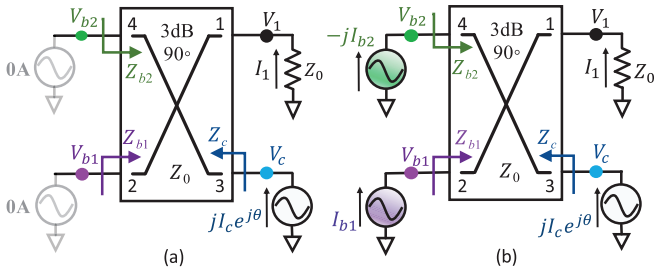

Fig. 2. Ideal generalized schematic of the output combining network for analyzing the proposed PD-ALMBA architecture. (a) $P_{OUT} < P_{max}/OBO$. (b) $P_{OUT} \geq P_{max}/OBO$.

with a developed PD-ALMBA prototype. With inherited wideband nature of PD-LMBA demonstrated in [29] and leveraging ultrawideband commercial quadrature couplers, and the advanced PD-ALMBA mode is physically realized over nearly unlimited bandwidth (two octaves in this design) with meanwhile ≥10-dB power back-off range. The theory and practical results presented in this article underline that the PD-ALMBA promises an ideal solution for developing next-generation ultrawideband and high-efficiency load-modulation PAs.

II. Asymmetrical LMBA Theory

Developed from the recently reported LMBA theory [21], a new architecture of asymmetrical LMBA is proposed in this section, and a generalized ALMBA theory framework is established.

A. Generalized Asymmetrical LMBA Mode

As shown in Fig. 1, the LMBA architecture [21] involves a BA and a CA combined with a predetermined phase offset. The behavior of LMBA can be modeled as three excitation sources driving the output quadrature coupler, and it is analytically described using impedance matrix given by

$$\begin{bmatrix} V_1 \\ V_2 \\ V_3 \\ V_4 \end{bmatrix} = Z_0 \begin{bmatrix} 0 & 0 & +j & -j\sqrt{2} \\ 0 & 0 & -j\sqrt{2} & +j \\ +j & -j\sqrt{2} & 0 & 0 \\ -j\sqrt{2} & +j & 0 & 0 \end{bmatrix} \begin{bmatrix} I_1 \\ I_2 \\ I_3 \\ I_4 \end{bmatrix} \tag{1}$$

where $V_1 = -I_1 Z_0$, $I_2 = I_{b1}$ and $I_4 = -jI_{b2}$ representing the input RF currents from BA1 and BA2, while $I_3 = jI_c e^{j\theta}$ denotes the CA current that is phase-shifted from BA1 by $\pi/2 + \theta$ [21], as shown in Fig. 2. Using the matrix operation illustrated in (1), the impedances of BA1 and BA2 can be calculated as

$$\begin{aligned} Z_{b1} &= Z_0 \left(\frac{I_{b2}}{I_{b1}} + \frac{\sqrt{2} I_c e^{j\theta}}{I_{b1}} \right) \\ Z_{b2} &= Z_0 \left(2 - \frac{I_{b1}}{I_{b2}} + \frac{\sqrt{2} I_c e^{j\theta}}{I_{b2}} \right). \end{aligned} \tag{2}$$

The load impedance seen by the CA can also be calculated from (1), given by

$$Z_c = Z_0 \left(1 - \sqrt{2} \frac{I_{b1} - I_{b2}}{I_c e^{j\theta}} \right). \tag{3}$$

An interesting fact is observed that the ALMBA described in (2) and (3) can be fully converged to the generic LMBA by setting $I_{b1} = I_{b2}$, in which BA1 and BA2 are loaded with the same impedance ($Z_{b1} = Z_{b2}$). Meanwhile, the CA in symmetrical LMBA is not load modulated regardless of the changes of currents. However, if BA1 and BA2 are not identical, the LM of CA can be achieved, while BA1 and BA2 are subject to different LM behaviors. By properly setting the phase and amplitude of all three amplifiers, their LM behaviors can be manipulated independently. This first-ever discovery leads to a generalization of the quadrature-coupler-based LM PA theory, and it fundamentally expands the design space of original LMBA.

B. Pseudo-Doherty Biasing and Current-Generator Modeling

By applying Doherty-like biasing of CA and BA, a PD-LMBA is constructed with CA as the carrier amplifier and BA as the peaking amplifier. As depicted in Fig. 2, the essence of PD-LMBA operation is based on the following conditions.

1) The BA1 and BA2 are turned off at low-power region where only the CA operates, as shown in Fig. 2(a);
2) When the CA reaches saturation ($I_c = I_{c,\max}$), the BA turns on at the same time, illustrated in Fig. 2(b).

Comparing with other LM technologies, the PD-LMBA architecture has three main advantages: 1) the power scaling between carrier and peaking amplifiers can be easily realized for achieving extended power back-off range, since the BA with two PAs combined is naturally stronger in power generation than the single branch of CA; 2) the optimal load modulation behavior of BA (purely resistive) can be achieved only with a static phase setting of CA which minimizes the complexity of phase control; and 3) under ideal phase and amplitude control, two efficiency peaks can be achieved at maximum power (P_{MAX}) and predefined OBO with minimal efficiency degradation in between. However, the CA in PD-LMBA reaches full saturation at the target OBO level, and, thus, it is under constant over-driving from OBO to P_{MAX}, resulting in linearity degradation and potential reliability issues of the entire PD-LMBA.

To alleviate the CA over-driving issue, a feasible solution is to enable LM on CA, which is similar to the carrier amplifier in distributed efficient PA (DEPA) [31], [32]. To better analyze the load-modulation characteristics of PD-ALMBA, the currents of BA1, BA2, and CA are carefully modeled [30]. As the carrier amplifier, the CA current, that is i_{ca}, is defined by

$$i_{\mathrm{ca}}(\beta) = \begin{cases} i_{\mathrm{ca,bo}}(\beta), & 0 \le \beta < \beta_{\mathrm{bo}} \\ i_{\mathrm{ca,h}}(\beta), & \beta_{\mathrm{bo}} \le \beta \le 1 \end{cases} \tag{4}$$

where $i_{\mathrm{ca,bo}}$ is the CA current at power back-off where the BA1 and BA2 are turned off, and $i_{\mathrm{ca,h}}$ denotes the CA current in high-power region where the BA1 and BA2 are turned on. β is the normalized variable to describe the magnitude of the input driving level, and β_{bo} is the threshold between the low-power and high-power regions. $i_{\mathrm{ca,bo}}$ can be simply expressed as the defined current of the ideal Class-B mode

$$i_{\mathrm{ca,bo}}(\beta) = \begin{cases} \dfrac{\beta}{\beta_{\mathrm{bo}}} \dfrac{I_{\mathrm{Max,C}}}{\alpha} \cdot \cos\theta, & -\frac{\pi}{2} \le \theta < \frac{\pi}{2} \\ 0, & \text{otherwise} \end{cases} \tag{5}$$

where $I_{\mathrm{Max,C}}$ represents the maximum current allowed to flow through the CA transistor, and α stands for the ratio between the maximum CA currents of low-power and high-power regions. It is interesting to note that α can also be considered as the LM ratio of CA. From (5), the dc and fundamental components of $i_{\mathrm{ca,bo}}$ can be obtained as

$$\begin{aligned} i_{\mathrm{ca,bo}}[0] &= \frac{2\beta}{\pi\alpha \cdot \beta_{\mathrm{bo}}} I_{\mathrm{Max,C}} \\ i_{\mathrm{ca,bo}}[1] &= \frac{\beta}{2\alpha \cdot \beta_{\mathrm{bo}}} I_{\mathrm{Max,C}}. \end{aligned} \tag{6}$$

When the driving power increases to β_{bo}, the CA is saturated corresponding to the first efficiency peak at the target OBO level. For symmetrical PD-LMBA ($\alpha = 1$) [28], [29], $i_{\mathrm{ca,bo}}$ grows to its maximum value, and this maximum CA current is maintained as the driving power continuing to increase toward the maximum input driving level ($\beta = 1$). For PD-ALMBA ($\alpha > 1$), the CA is only voltage saturated at β_{bo}, which still leads to an efficiency peak, and the CA current is increased by a factor of α to the full saturation (both voltage and current) at $\beta = 1$. Therefore, $i_{\mathrm{ca,h}}$ of PD-ALMBA can be expressed as

$$i_{\mathrm{ca,h}}(\beta) = \begin{cases} I_{\mathrm{Max,C}} \cdot \cos\theta, & -\dfrac{\pi}{2} \le \theta < \dfrac{\pi}{2} \\ 0, & \text{otherwise.} \end{cases} \tag{7}$$

The fundamental component of CA current (I_{ca}) is plotted as the blue curve in Fig. 3. With a variation of LM factor, i.e., $\alpha \in (1, 2)$, the CA LM falls within a continuum between symmetrical PD-LMBA and DPA.

The BAs are biased identically at Class-C mode. Assuming that i_{b1} and i_{b2} are proportional, they can be derived as

$$i_{\mathrm{ba1}}(\beta) = \begin{cases} 0, & 0 \le \beta < \beta_{\mathrm{bo}} \\ i_{\mathrm{ba1,h}}(\beta), & \beta_{\mathrm{bo}} \le \beta \le 1 \end{cases} \tag{8}$$

$$i_{\mathrm{ba2}}(\beta) = \sigma \cdot i_{\mathrm{ba1}}(\beta) \tag{9}$$

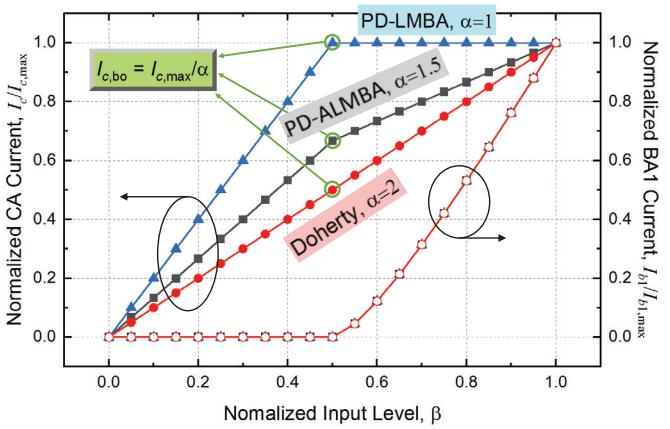

Fig. 3. Normalized currents of I_c and I_{b1} when $\beta_{\mathrm{bo}} = 0.5$ for different PA modes, i.e., PD-LMBA, PD-ALMBA, and DPA.

where σ represents the current scaling ratio between BA1 and BA2 (e.g., $\sigma = 1$ for symmetrical BA). The BA1 current in high-power region can be expressed using Class-C current formula as

$$i_{\mathrm{ba1,h}}(\beta) = \begin{cases} \dfrac{\beta \cdot \cos\theta - \beta_{\mathrm{bo}}}{1-\beta_{\mathrm{bo}}} I_{\mathrm{Max,B1}}, & -\theta_b \le \theta < \theta_b \\ 0, & \text{otherwise} \end{cases} \tag{10}$$

where $(-\theta_b, +\theta_b)$ defines the turn-on phase range of BA1 and BA2. Thus, θ_b is obtained as

$$\theta_b = \arccos(\beta_{\mathrm{bo}}/\beta). \tag{11}$$

By applying Fourier Transformation, the dc and fundamental currents of BA1 can be calculated as

$$\begin{aligned} i_{\mathrm{ba1,h}}[0] &= \frac{I_{\mathrm{Max,B1}}}{1-\beta_{\mathrm{bo}}} \cdot \frac{2\beta\sin\theta_b - 2\beta_{\mathrm{bo}}\theta_b}{\pi} \\ i_{\mathrm{ba1,h}}[1] &= \frac{I_{\mathrm{Max,B1}}}{1-\beta_{\mathrm{bo}}} \cdot \frac{\beta(2\theta_b + \sin 2\theta_b) - 4\beta_{\mathrm{bo}}\sin\theta_b}{2\pi}. \end{aligned} \tag{12}$$

The normalized current of the BA1 versus β is presented in Fig. 3. The BA current is only dependent on the driving level, β, regardless of CA LM factor, α.

C. Load Modulation Analysis of PD-ALMBA

For PD-ALMBA, the CA is load modulated after the CA first reaches voltage saturation at the predefined OBO with a decreasing Z_c and an increasing I_c, thus extending the linear range of CA. Realistically, this can be achieved by enforcing asymmetry between BA's two sub-amplifiers, that is the difference of current between BA1 and BA2, as indicated by (3). To theoretically analyze the PD-ALMBA, its operation is divided into the following three regions.

1) *Low-Power Region ($P_{\mathrm{OUT}} < P_{\mathrm{MAX}}/\mathrm{OBO}$):* When operating at low-power level below the predefined target OBO power, the BA1 and BA2 are completely turned off, as depicted in Fig. 2(a). The CA operates as a standalone Class-AB amplifier, and the output power is solely generated by CA. In this back-off region, the LM behaviors of BA1 and BA2 as well as the CA impedance are provided as follows:

$$\begin{aligned} Z_{b1,\mathrm{LP}} &= Z_{b2,\mathrm{LP}} \\ &= \infty \\ Z_{c,\mathrm{LP}} &= Z_0. \end{aligned} \tag{13}$$

The currents, I_{b1}, I_{b2}, and I_c, can be expressed as

$$\begin{aligned} I_{b1} &= I_{b2}/\sigma \\ &= 0 \\ I_c &= (I_{c,\mathrm{bo}}/\beta_{\mathrm{bo}}) \cdot \beta. \end{aligned} \tag{14}$$

Since BAs are turned off, the efficiency of overall PD-LMBA is equal to the efficiency of the CA.

2) *LM Region ($P_{\mathrm{MAX}}/\mathrm{OBO} \le P_{\mathrm{OUT}} < P_{\mathrm{MAX}}$):* When the power increases to the target OBO level, the BA1 and BA2 are turned on, and the CA reaches saturation at the same time. At $P_{\mathrm{MAX}}/\mathrm{OBO}$, the CA is designed to be only voltage-saturated ($Z_c > Z_{\mathrm{CA,Opt}}$) corresponding to the first efficiency peak, while there is still headroom for further increase of CA current. In this region, BA1 and BA2 currents increase proportionally given by

$$\begin{aligned} I_{b1} &= i_{\mathrm{ba1,h}}[1] \\ I_{b2} &= \sigma \cdot i_{\mathrm{ba1,h}}[1]. \end{aligned} \tag{15}$$

By substituting this dependence into (2) and (3), the load modulation behaviors of BA1, BA2, and CA impedances are derived as

$$\begin{aligned} Z_{b1,\mathrm{LM}} &= Z_0\left(\sigma + \frac{\sqrt{2}I_c e^{j\theta}}{I_{b1}}\right) \\ Z_{b2,\mathrm{LM}} &= Z_0\left(\left(2 - \frac{1}{\sigma}\right) + \frac{\sqrt{2}I_c e^{j\theta}}{\sigma I_{b1}}\right) \\ Z_{c,\mathrm{LM}} &= Z_0\left(1 - \frac{\sqrt{2}I_{b1}(1-\sigma)}{I_c e^{j\theta}}\right). \end{aligned} \tag{16}$$

The above equation clearly underlines that by setting $\sigma < 1$ (larger BA1 sizing), Z_c can be modulated below Z_0 as the power increases beyond OBO. Such a decreasing Z_c is achieved given the fact that BA1 current (I_{b1}) rises much more sharply after turning on as compared to I_c (i.e., I_{b1}/I_c increases with power). Meanwhile, due to the CA LM, the CA current at the predefined OBO ($I_{c,\mathrm{bo}}$) is expected to gradually increase to the full current saturation, that is $I_{c,\max} = \alpha I_{c,\mathrm{bo}}$. Similar to the DEPA [32], this LM-induced CA current increase is assumed to be linearly dependent on the driving level, β, given by

$$I_c = I_{c,\mathrm{bo}}\left(\frac{\alpha - 1}{1-\beta_{\mathrm{bo}}}\beta + \frac{1-\alpha\beta_{\mathrm{bo}}}{1-\beta_{\mathrm{bo}}}\right). \tag{17}$$

The CA current with a reduced carrier LM ratio of $\alpha = 1.5$ is plotted in Fig. 3. Compared to DPA with full LM ratio of $\alpha = 2$, the CA current of PD-ALMBA increases with different slopes in different regions.

3) *Saturation Region ($P_{\mathrm{OUT}} = P_{\mathrm{MAX}}$):* When the output power reaches the maximum, CA and BA are fully saturated at the same time. The currents of all amplifiers reach to their maximum value, which can be expressed as

$$\begin{aligned} I_{b1} &= I_{b1,\max} \\ I_{b2} &= \sigma \cdot I_{b1,\max} \\ I_c &= I_{c,\max} \\ &= \alpha \cdot I_{c,\mathrm{bo}}. \end{aligned} \tag{18}$$

In this saturated region, I_c will expand to $\alpha \cdot I_{c,\max}$ due to CA-LM. Since CA bias voltage remains constant, Z_c will decrease from Z_0 to Z_0/α. The load impedances of BA1, BA2, and CA are given by

$$\begin{aligned} Z_{b1,\mathrm{SAT}} &= Z_0\left(\sigma + \frac{\sqrt{2}I_{c,\max}e^{j\theta}}{I_{b1,\max}}\right) \\ Z_{b2,\mathrm{SAT}} &= Z_0\left(\left(2 - \frac{1}{\sigma}\right) + \frac{\sqrt{2}I_{c,\max}e^{j\theta}}{\sigma I_{b1,\max}}\right) \end{aligned}$$

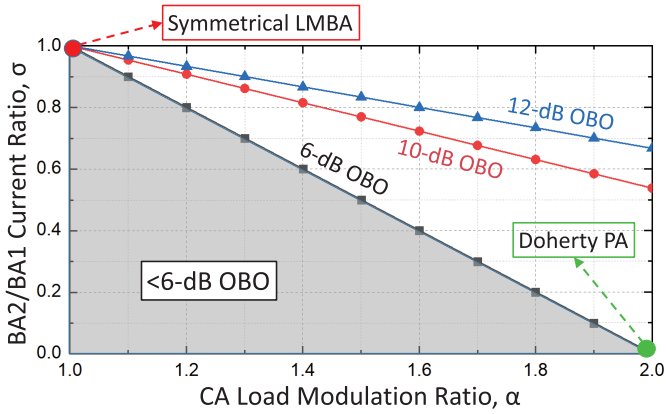

Fig. 4. Dependence between σ and α various given target OBO.

$$Z_{c,\mathrm{SAT}} = Z_0\left(1 - \frac{\sqrt{2}I_{b1,\max}(1-\sigma)}{I_{c,\max}e^{j\theta}}\right) = \frac{Z_0}{\alpha}. \tag{19}$$

It is interesting to note that the carrier LM of PD-ALMBA can be set as a continuum between PD-LMBA ($\alpha = 1$) and DPA ($\alpha = 2$), depending on the target need for over-driving reduction of CA and the overall PD-ALMBA performance. Based on the above theoretical analysis, the amplitude and phase control between three amplifiers, that is BA1, BA2, and CA, govern their LM behaviors and the general operation of the PD-ALMBA, which will be analyzed in detail in the following Section II-D.

D. Amplitude and Phase Control of PD-ALMBA

Different from the generic LMBA, the amplitude control of ALMBA involves not only the BA-CA scaling (I_c/I_{b1}) but also the BA1-BA2 scaling (σ), as indicated by (16). In the PD-ALMBA operation, BA1 and BA2 need to be turned on at a predetermined back-off power, where CA reaches its voltage saturation. After all amplifiers are fully saturated, the total saturation power in combination of BA1, BA2, and CA should be scaled proportionally, that is $\mathrm{OBO_{dB}}$ dB higher than the back-off level. Based on the ideal model in Fig. 2, the power scaling ratio between BA1, BA2, and CA can be determined by

$$\frac{1}{2}\mathrm{OBO}\cdot\left(\frac{I_{c,\max}}{\alpha}\right)^2\cdot Z_0 = \frac{1}{2}I_{c,\max}^2\cdot\frac{Z_0}{\alpha} + \frac{1}{2}I_{b1,\max}^2\cdot R_{b1,\mathrm{sat}} + \frac{1}{2}I_{b2,\max}^2\cdot R_{b2,\mathrm{sat}}. \tag{20}$$

The dependence between σ and α under different target OBO ranges can be derived with a combination of (19), (18), and (20), and the results are graphically presented in Fig. 4. As an interesting phenomenon observed in Fig. 4, $I_{b2} = 0$ is required to result in 6 dB of OBO and 2 of LM ratio, indicating the fact that the PD-ALMBA is converged to a standard DPA with the quadrature coupler functioning as an ideal Doherty combiner [33]. The upper right half region of Fig. 4 marks the extended

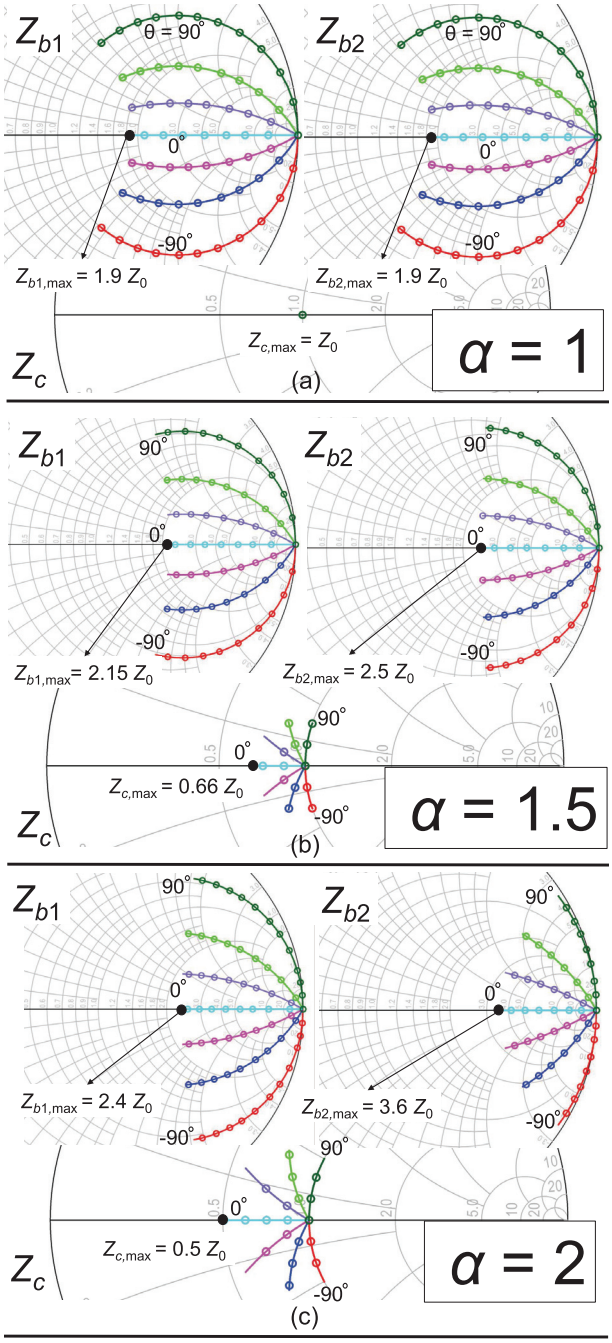

Fig. 5. Continuum of BA1, BA2, and CA LMs using the ideal generalized model for OBO = 10 dB and various CA-LM ratio, α. (a) when α is set to 1. (b) when α is set to 1.5. (c) when α is set to 2.

OBO range (>6 dB) that can be utilized in practical designs for amplification of high-PAPR signals.

In addition to amplitude control, it is necessary to ensure that the phase difference between the current generators is properly set to result in optimal LM trajectories of each amplifier. As described in (16), by setting $\theta = 0$, a purely resistive LM of Z_{b1}, Z_{b2}, Z_c can be achieved, which represents the optimal LM behavior according to the load-line theory [34]. Fig. 5 shows the analytically calculated LM trajectories of BA1, BA2, and CA for variations of phase offset (θ) and CA LM ratio (α) under a constant OBO of 10 dB. All the LM traces can be maintained on the real axis of Smith

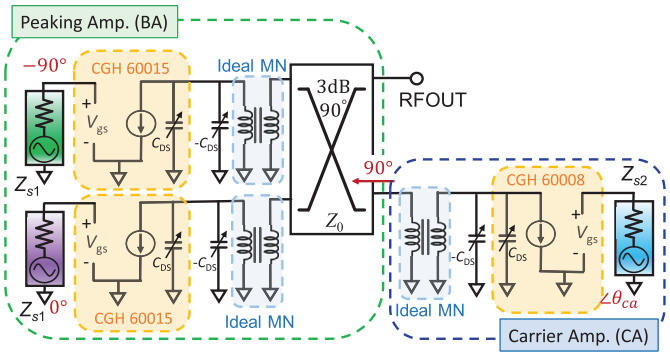

Fig. 6. Emulated model setup of the proposed PD-ALMBA with bare-die GaN transistors.

chart for $\theta = 0$. In realistic design with matching networks and parasitics of transistors, the optimal BA-CA phase offset will be determined through exhaustive sweeping in the actual circuit schematic.

In summary, this section articulates a unified theory of quadrature-coupler-based amplifier with active LM of three different driving sources. The equations derived in this section prove that the asymmetry between BA1 and BA2 not only maintains the validity of LMBA architecture in Fig. 2 but also leads to a continuum LM ratio of CA. Moreover, the LM of BA1, BA2, and CA can be performed individually in this PD-ALMBA topology, which is able to inherit the wideband and high-efficiency characteristics of symmetrical PD-LMBA. Meanwhile, the reduced CA over-driving leads to promising potential of improved linearity and reliability.

III. Verification Using Emulated Ideal PD-ALMBA Model

To verify the PD-ALMBA theory proposed in Sec. II, an ideal PD-ALMBA is emulated using bare-die GaN transistors and ideal quadrature coupler. The bare-die devices have minimized parasitics, which can closely mimic the behaviors of the ideal current generators in Fig. 2.

A. Emulation of Ideal PD-ALMBA Model

Two different types of bare die transistors are used to establish the emulated ideal PD-ALMBA, as shown in Fig. 6. Specifically, BA1 and BA2 are built with CGH60015 model from Wolfspeed. The intrinsic parasitic capacitance of the transistors ($C_{\rm DS}$) is de-embedded using a dedicated negative capacitance, $-C_{\rm DS}$. Therefore, the combo of transistor and $-C_{\rm DS}$ can emulate an ideal current source. The input impedances for BA1 and BA2 are set to Z_{s1} obtained using the source-pull. Due to the LM of CA as derived in (19), the impedances of BA1 and BA2 at saturation power (i.e., $Z_{b1,\rm sat}$ and $Z_{b2,\rm sat}$) are different from the coupler characteristic impedance ($Z_0 = 50\ \Omega$). To study the continuum of LM behavior (α from 1 to 2), the transformer design is based on the symmetrical case ($\alpha = 1$) in which $Z_{b1,\rm sat}$ and $Z_{b2,\rm sat}$ are matched to $R_{\rm Opt}$ of the transistor. Then, the power asymmetry

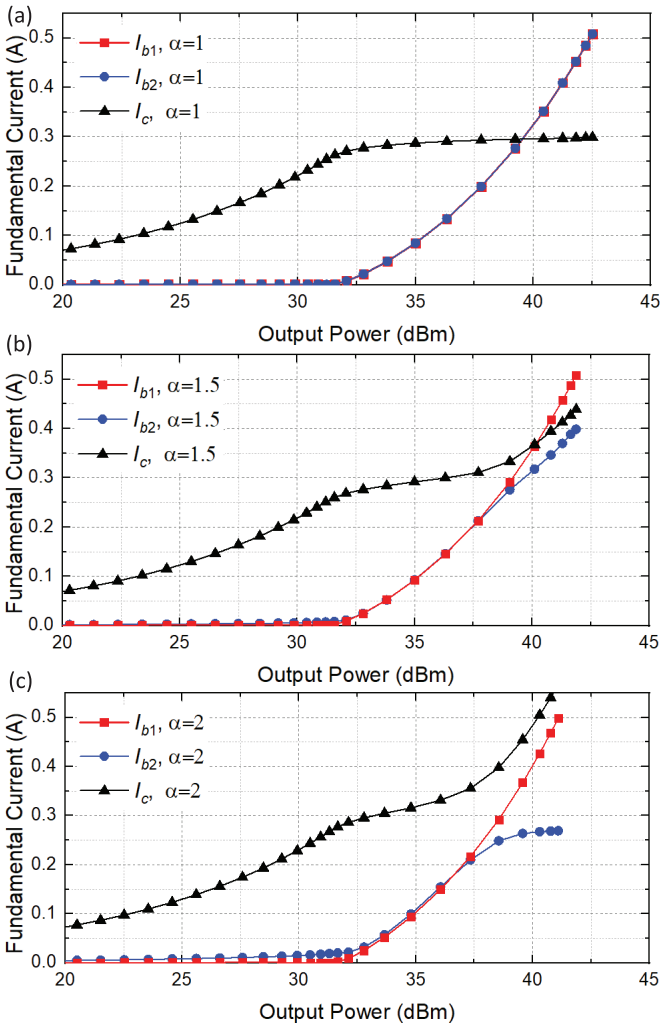

Fig. 7. Simulated BA1, BA2, and CA currents using emulated PD-ALMBA model at 1.7 GHz for different LM ratios. (a) $\alpha = 1$. (b) $\alpha = 1.5$. (c) $\alpha = 2$.

of BA1 and BA2 (i.e., $\sigma < 1$) is realized by offsetting the bias voltages of BA1 and BA2 for practically achieving $\alpha > 1$. The output of CA is connected to the isolation port of the coupler. Considering that the output power of CA is much less than the total output power of BA, the bare-die CGH60008 model from Wolfspeed is selected with a smaller device size. The input impedance of CA is set to Z_{s2}, which is obtained from source-pull simulation result. Due to the fact that the CA impedance is modulated from Z_0 to Z_0/α at the coupler interface, the same LM range is transformed to CA transistor by another ideal transformer with optimized transformation ratio based on the CA power and bias voltage. It turns out that the CA transistor with reduced $V_{\rm DD}$ desires $R_{\rm Opt,CA} \approx Z_0$, leading to a 1:1 transformer for CA.

According to Fig. 2 and (13), the ideal phase offset between BA1 (I_{b1}) and the control source power (CSP, $jI_ce^{j\theta}$) is 90° at the coupler interface plane, such that the resistive LM can be achieved by setting $\theta = 0°$. Therefore, the CA input phase ($\theta_{\rm CA}$) needs to be properly selected to ensure that a 90° phase offset is maintained at the coupler interface for BA1 path and CA path.

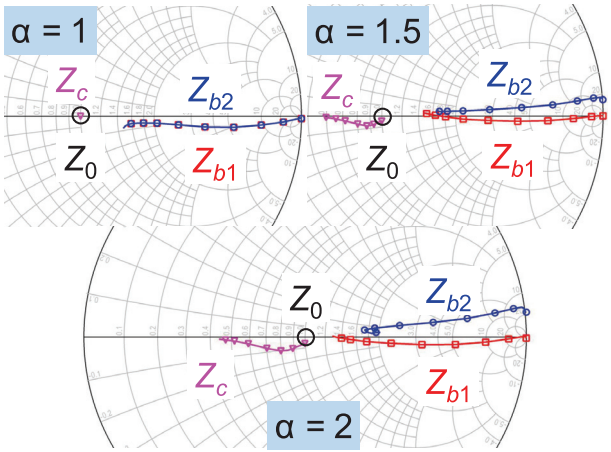

Fig. 8. Simulated BA and CA LM trajectories of different α at 1.7 GHz using emulation PD-ALMBA model.

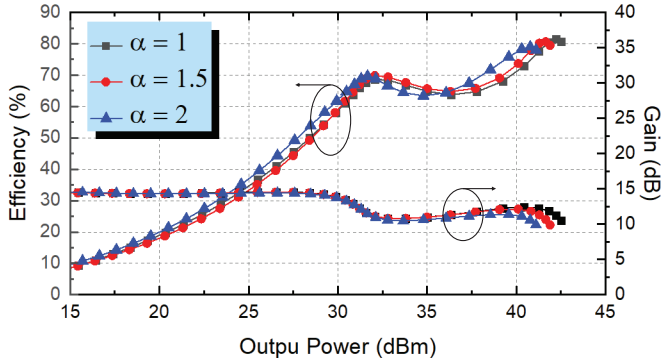

Fig. 9. Simulated power-swept efficiency of different α at 1.7 GHz.

B. Simulation Results

Fig. 7 shows the simulated fundamental current of the PD-ALMBA emulated model with different α values. The simulation results in Fig. 7(a) clearly show that when I_{b1} and I_{b2} are identical, α is equal to 1, and the CA remains in the saturation region with constant I_c beyond the back-off point. However, for $I_{b1} > I_{b2}$, α becomes greater than 1, and I_c continues to increase after turning-on of BA, shown in Fig. 7(b) and (c). This PD-ALMBA model is able to alleviate the over-driving problem of CA. On the other hand, an excessively large value of α may also cause adverse effects for identical matching of BA1 and BA2. As observed in Fig. 7(c) with $\alpha = 2$, I_{b2} reaches saturation earlier than BA1, which may cause over-driving of BA2. While this can be solved by designing different transformers to BA1 and BA2, it may complicate the design since different matching networks can have different frequency response. Therefore, in actual circuit design in this article, $\alpha \approx 1.5$ is selected as the sweep spot of CA LM ratio.

Fig. 8 shows the emulated model load trajectory of BA1, BA2, and CA with various α at 1.7 GHz. As seen from the figure, when $\alpha = 1$, Z_c equal to Z_0, and the maximum values of Z_{b1} and Z_{b2} are equal; when α is greater than 1, Z_c is modulated along a resistive load trajectory in which the impedance decreases from Z_0 to Z_0/α, while $Z_{b2,\mathrm{Sat}}$ is greater than $Z_{b1,\mathrm{Sat}}$. The simulation results are consistent with the theoretical derivation in Sec. II, solidly proving the proposed ALMBA/PD-ALMBA theory. Fig. 9 shows the simulated efficiency of different emulation models with different α at 1.7 GHz. The results show that the increase of LM ratio (α) does not affect the overall output efficiency and gain on the basis of reducing CA over-driving.

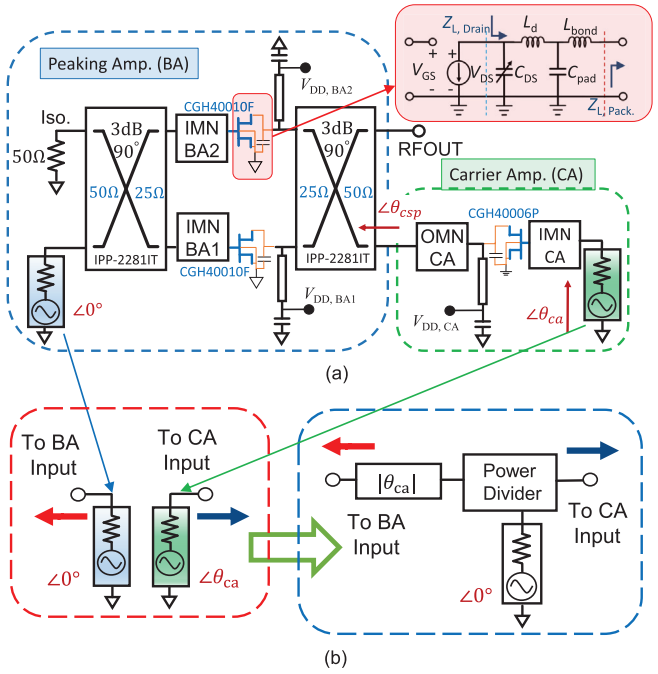

Fig. 10. (a) Simulation setup of the proposed PD-ALMBA using realistic GaN transistors de-embedded with parasitic networks. (b) Design of TL-based wideband phase shifter for merging the BA and CA inputs.

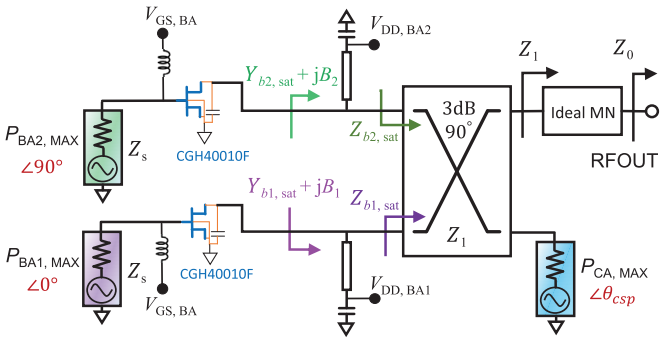

Fig. 11. BA matching design at maximum power.

IV. Practical Design of Ultrawideband PD-ALMBA

Based on the PD-ALMBA theory and emulation presented in Secs. II and III, the LM ratio of CA, α, is directly related to the asymmetry of BA1 and BA2, σ, and the target OBO range. Considering the sweet spot of PD-ALMBA operation, a reduced CA LM ratio of $\alpha = 1.5$ is targeted in the practical design [17]. To accommodate the high PAPR of emerging 4G and 5G signals, the target OBO is set to 10 dB. Two 10-W commercial GaN HEMTs (Wolfspeed CGH40010F) are

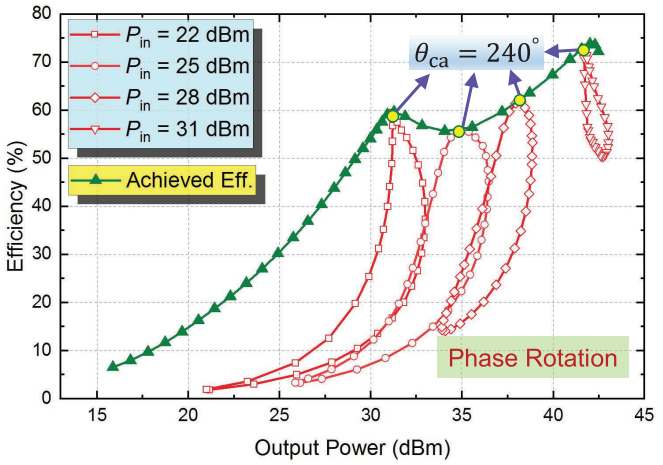

Fig. 12. Determination of the optimal BA-CA phase offset based on dual-input circuit schematic in Fig. 6 at 1.0 GHz through phase-swept input stimulus of CA.

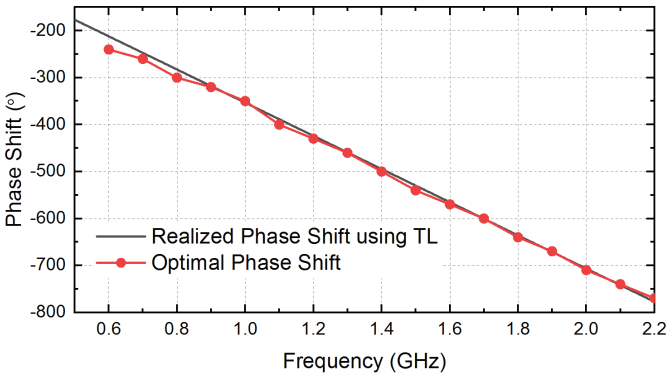

Fig. 13. Simulated optimal BA1-CA phase offset at different frequencies.

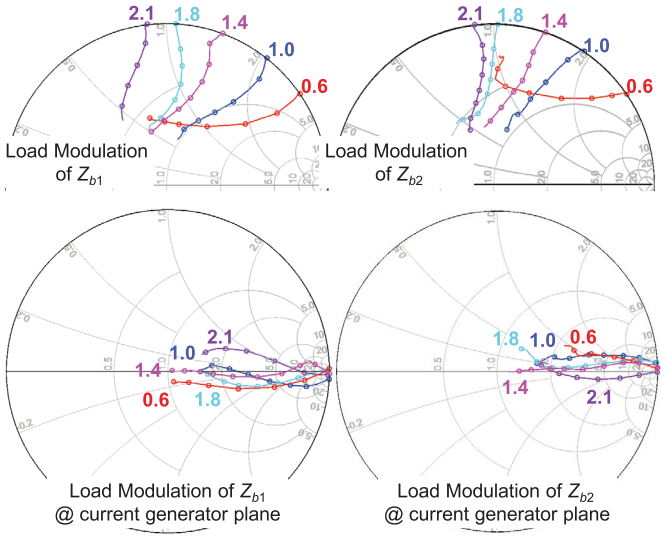

Fig. 14. LM of Z_{b1} and Z_{b2} across the entire bandwidth for $\alpha = 1.5$.

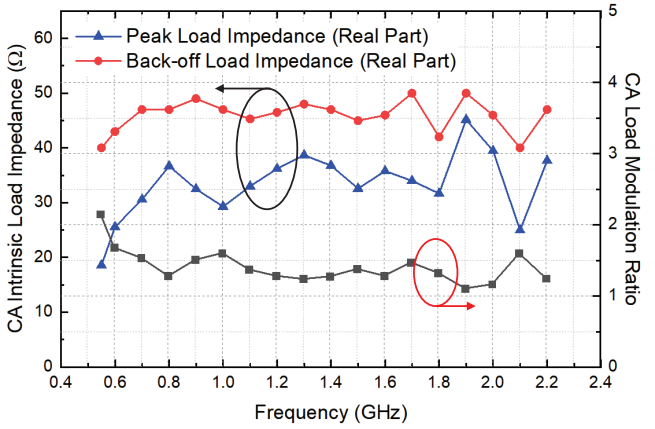

Fig. 15. Simulated CA load-modulation behavior across the entire frequency band.

used as the active devices for both BA1 and BA2, which are combined through two commercial quadrature couplers (IPP-2281IT from Innovative Power Products). To achieve the target CA modulation, the BA2 power is down-scaled from BA1 by reducing the BA2 supply voltage, which is finally determined through circuit simulation. Due to the fact that the CA power is much lower as compared to BA, the physical circuit of CA is constructed using a 6-W GaN transistor (Wolfspeed CGH40006P), while the CA power is practically controlled with reduced $V_{DD,CA}$ in the actual circuit. The overall realized circuit schematic is shown in Fig. 10(a). The target frequency range is 0.55 to 2.2 GHz, covering a majority of cellular communications bands.

A. Design of Asymmetrical Balanced Amplifier

Using a similar approach as presented in [28], [29], and [35], the wideband matching for the transistor is primarily realized with a wideband non-50-Ω quadrature coupler and a bias line. As the schematic shown in Fig. 10, this circuit implementation of BA eliminates the complex wideband output matching network, resulting in minimized dispersion effect and simplified load-modulation control.

A fact is noted that the packaged GaN transistor (e.g., CGH40010F) desires a nearly constant real part of load admittance ($Y_L = G_L + jB_L$) over wide frequency range extracted from the load-pull simulation, also seen in [36]–[38]. According to the expressions of $Z_{b1,sat}$ and $Z_{b2,sat}$ in (19), BA1 and BA2 see different impedances at the quadrature coupler plane with the contribution of CA. Therefore, to determine the characteristic impedance of the quadrature coupler, Z_1, co-simulation with CA is needed, which is modeled as an ideal source (CSP) with maximum CA power $P_{CA,MAX}$ ($=\alpha P_{MAX}/OBO$ as for estimation) at a proper phase. Z_1 is optimized such that $Y_{b1,sat}$ and $Y_{b2,sat}$ are both close to $G_{L,Opt}$. Since BA1 generates the highest power, the optimization of $Y_{b1,sat}$ is given higher priority. The bias-line parameters (i.e., length and width) are utilized to provide dedicated values of B_L for BA1 and BA2 over the target frequency range. The detailed design procedure is described in Fig. 11. The circuit simulation results show that Z_1 of 20–30 Ω is the optimal value for covering the target frequency range. Therefore, a wideband impedance-transformer (2:1) coupler (IPP-2281IT,

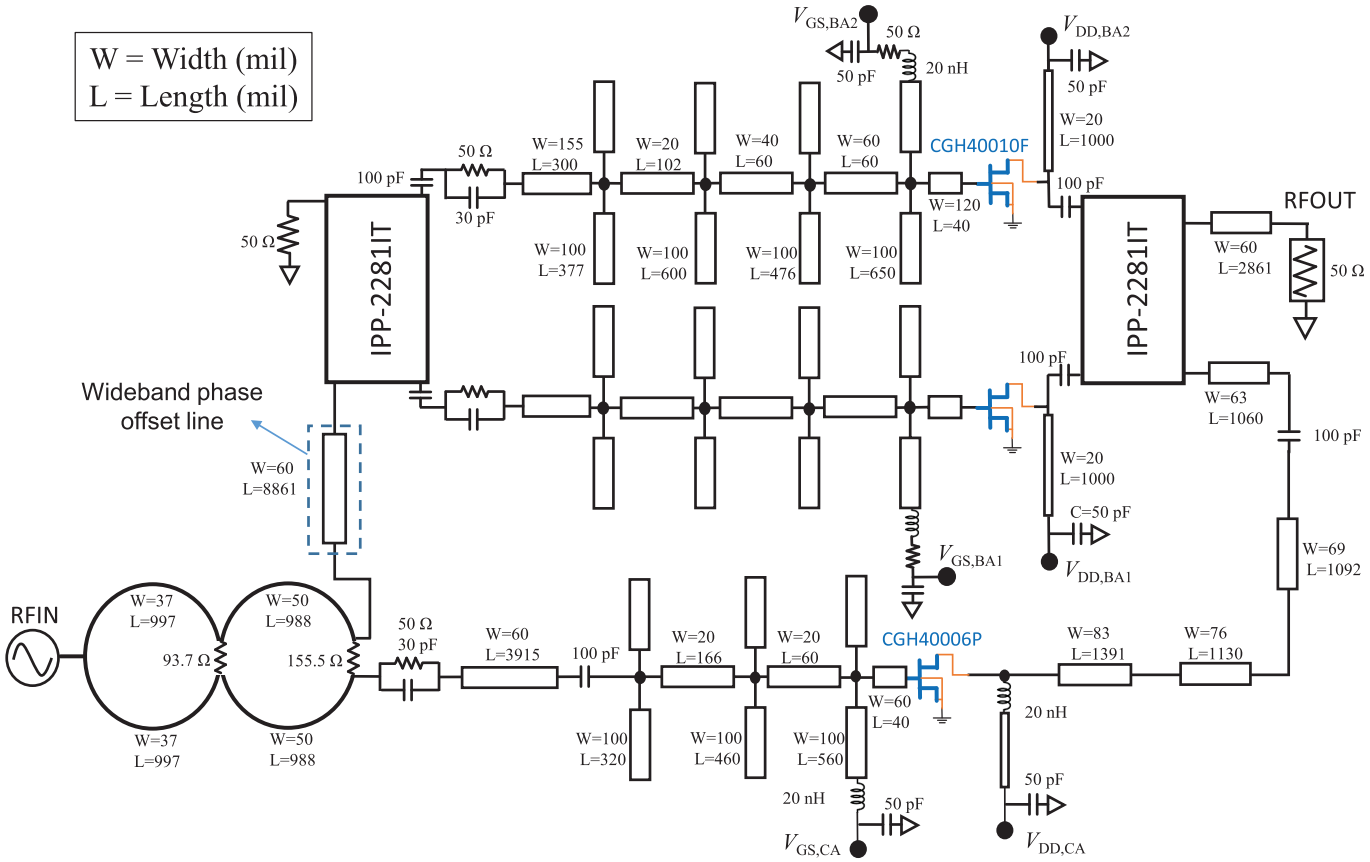

Fig. 16. Circuit schematic overview of designed PD-LMBA.

commercially available from Innovative Power Product) is utilized to provide the desired BA matching.

The same transformer coupler is used for the input quadrature division of BA, leading to an eased transformation ratio of input matching, that is from 25 Ω to the designated source impedance Z_s. The physical matching circuit is realized using the multistage lowpass matching network and design method introduced in [36]. Since this design has two octave bandwidths, half of the frequencies have second harmonics in band; therefore, we did not specifically design for harmonic termination but rely on saturation-mode for harmonic shaping [5]. On the other hand, BA1 and BA2 in Class-C mode are already more efficient than CA in Class-AB, so the harmonic matching is not necessary for BAs.

B. Design of Control Amplifier

According to the amplitude control scheme described in Secs. II and III, the OBO power of CA determines the dynamic range once the BA design is fixed. Given a specific OBO, the saturation power of CA can be determined by

$$\text{OBO} \times \frac{P_{\text{CA,MAX}}}{\alpha} = P_{\text{BA1,MAX}} + P_{\text{BA2,MAX}} + P_{\text{CA,MAX}}. \tag{21}$$

To achieve the target OBO of 10 dB, $P_{\text{CA,MAX}}$ should be around 7.5-dB below $P_{\text{BA1,MAX}} + P_{\text{BA2,MAX}}$. To realize this low output power, the CA is implemented with a 6-W GaN transistor (Wolfspeed CGH40006P), and it is biased in Class-AB mode with partial V_{DD}.

Since the CA is connected to the isolation port of the transformer coupler, the CA design is based on the 50-Ω reference impedance. With the target LM ratio of α set to 1.5, Z_c (at the coupler plane) should be modulated from 50 to 33 Ω as the power increases from 10-dB OBO to maximum, shown in Fig. 5(b). The LM ratio of CA (α) is determined by the asymmetry of BA1 and BA2, which is practically realized using the combination of: 1) fluctuation of quadrature coupler's transmission/coupling coefficients over frequency that is inevitable for wideband couplers, and 2) reduction of BA2 bias voltage. Thus, output matching of CA is required to transform this LM behavior from the coupler plane to the transistor package plane and eventually to the intrinsic drain plane. In the actual design of this article, a three-section transmission line matching network is designed, and the CA matching is eventually optimized through co-simulation with the designed BA.

The input matching network design of CA followed the same methodology as wideband input design of BA1 and BA2, and a three-section lowpass network based on transmission lines is designed to provide wideband input matching for the selected GaN transistor. Considering the complexity of the design and the dual-octave bandwidth, the harmonic control circuitry is not particularly included in this work. However,

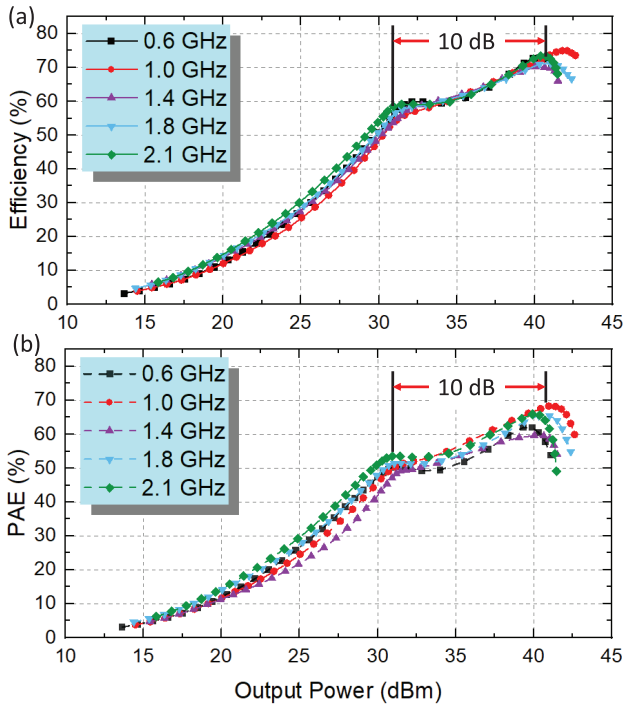

Fig. 17. Power-swept CW simulation results of the designed PD-ALMBA with the best BA-CA phase setting at different frequencies. (a) Drain efficiency. (b) PAE.

if certain harmonic matching is involved in CA design, it can potentially further improve the PD-ALMBA OBO efficiency.

C. BA-CA Phase Offset Design Over Ultrawide Bandwidth

After finishing the design of BA1, BA2, and CA, the LM of all three amplifiers is mainly determined by the relative phase between BA1 and CA, as described in (16). To ensure the resistive LM of BA1, BA2, and CA for maximized back-off efficiency, the BA1-CA phase offset is required to be $\theta = 0°$ (equivalent to $\theta_{\mathrm{CSP}} = 90°$) at the coupler plane. With the practical BA and CA incorporated with the coupler, the phase offset optimization is moved to the inputs of BA and CA, which can be determined using the dual-input (with equal amplitude [27]) schematic shown in Fig. 12. It is worth noting that the optimal phase shift between BA and CA is almost linearly proportional to the frequency with a negative slope, as plotted in Fig. 13. Therefore, a 50-Ω transmission line (TL) can be used to achieve this frequency-dependent phase shift [28], [29], [35], thereby providing accurate wideband phase control. Given the fact that the relative phase between CA and BA is negative, the offset transmission line in the CA path has a negative length, and it is functionally equivalent to placing a symmetrical TL with a positive length in the BA path. Using this TL phase shifter, and a standard wideband Wilkinson frequency divider can combine the dual inputs to a single RF input, as depicted in Fig. 10(b).

To verify the wideband LM behaviors of all three amplifiers, the transistor parasitic network is modeled to access the intrinsic drain LM trajectory at the current generator plane, as shown in Fig. 14. The desired resistive LM trajectories

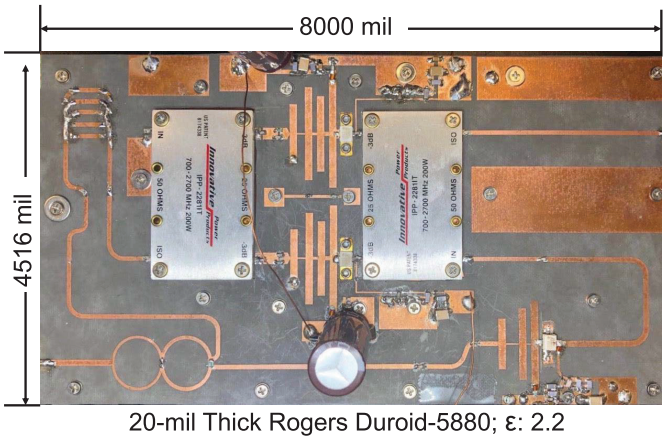

Fig. 18. Fabricated PD-ALMBA prototype.

are achieved for BA1 and BA2 over the entire frequency range. The optimized real part impedances of CA (for P_{MAX} and OBO) at the intrinsic drain plane are shown in Fig. 15, indicating that the target LM ratio of 1.5 can be achieved across the target band. The CA-LM trajectory travels nearly on the real axis with very small fluctuations, as shown in Fig. 8, so the imaginary part changes of CA are ignored.

D. Overall Schematic and Simulation Results

The finalized circuit schematic of overview is shown in Fig. 16, all actual circuit-element values are exhibited next to the schematic. The gate bias voltages of BA1 and BA2 are properly set such that they turn on around 10 dB power back-off, where the CA LM is performed concurrently.

Through the design of the wideband BA1, BA2, CA, and phase shifter described in above sections, the overall efficiency and PAE of the PD-ALMBA are simulated with swept input power, as shown in Fig. 17. It is clearly seen that a high efficiency is achieved at the peak power, and the back-off efficiency is significantly enhanced down to 10-dB OBO. This Doherty-like efficiency and PAE profile can be well-maintained overextended frequency range.

V. Implementation and Experimental Results

The PD-ALMBA is implemented on a 20-mil thick Rogers Duroid-5880 PCB board with a dielectric constant of 2.2. A photograph of the fabricated PD-ALMBA is shown in Fig. 18. The size of the entire circuit is 4.5 in × 8 inch. The fabricated PD-ALMBA is measured using both continuous-wave (CW) and modulated LTE signals. In this implemented circuit, CA is biased in Class-AB with a $V_{\mathrm{DD,CA}}$ around 11 V. BA1 and BA2 are biased in Class-C with 32-V $V_{\mathrm{DD,BA1}}$ and 24-V $V_{\mathrm{DD,BA2}}$, respectively. Fine tuning of $V_{\mathrm{GS,BA1}}$ and $V_{\mathrm{GS,BA2}}$ between -5 and -4 V is performed at different frequencies to optimize the best power-added efficiency (PAE). Fig. 19 shows drain dc currents versus output power from CW measurement for BA1, BA2, and CA, where a comparison is experimentally presented between symmetrical and asymmetrical cases. It can be clearly seen from Fig. 19(b) that the current of CA continuously increasing after the turning-on of

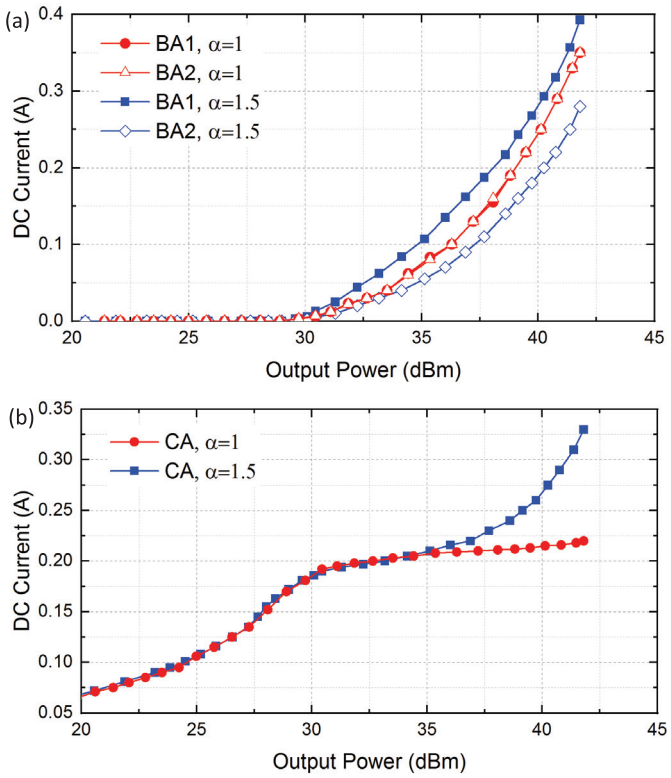

Fig. 19. Measured drain dc current versus output power of BA1, BA2, and CA at 1.4 GHz. (a) when α is set to 1. (b) when α is set to 1.5.

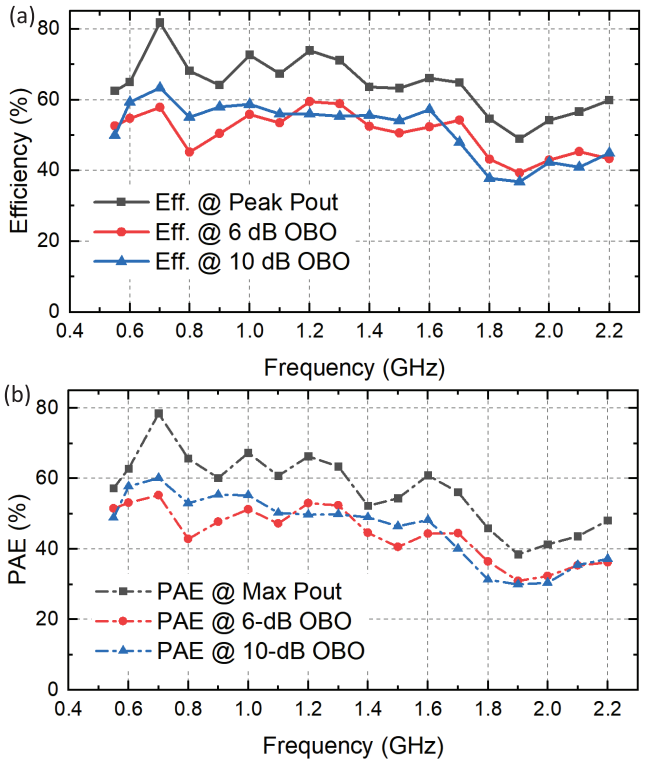

Fig. 21. (a) Measured drain efficiency at various OBO levels from 0.55 to 2.2 GHz. (b) Measured PAE at various OBO levels from 0.55 to 2.2 GHz.

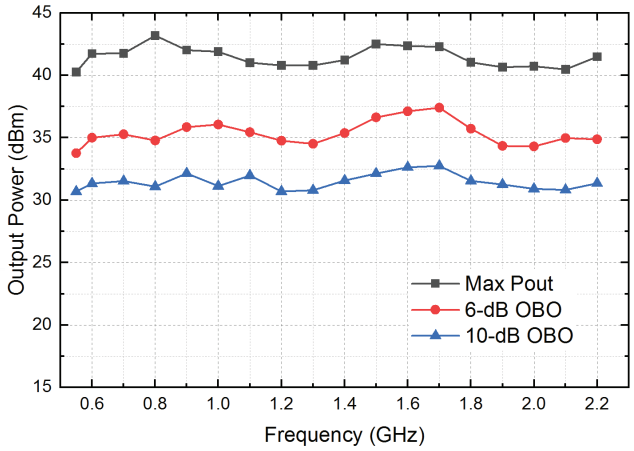

Fig. 20. Measured output power at various OBO levels from 0.55 to 2.2 GHz.

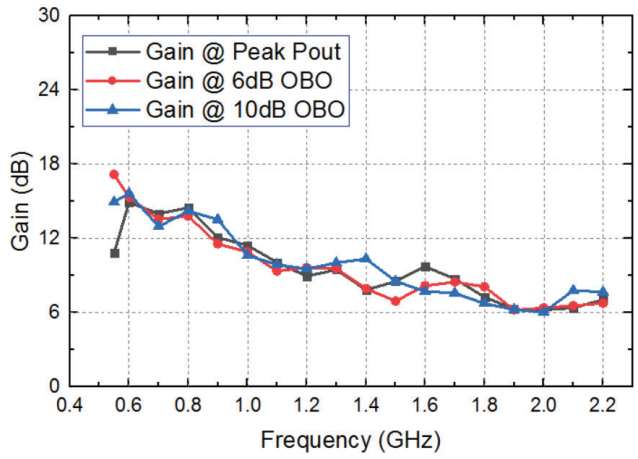

Fig. 22. Measured gain at various OBO levels from 0.55 to 2.2 GHz.

BA for ALMBA. These results exhibit a solid validation of the propose ALMBA theory and well agree with the simulated fundamental currents using emulation model in Fig. 7.

A. Continuous-Wave Measurement

The fabricated PD-ALMBA is measured under the excitation of a single-tone CW signal from 0.55 to 2.2 GHz with a large variation of power levels. The CW signal is generated by a vector signal generator, and then boosted by a broadband linear driver amplifier to a sufficiently high level for driving the device under test (DUT). The output power is measured using spectrum analyzer and power sensor. A peak output power of 41–43 dBm is measured across the entire bandwidth, as shown in Fig. 20. In Fig. 21, 82% of drain efficiency and 79% of PAE at peak power is measured at 0.7 GHz. The drain efficiency remains higher than 49% and PAE remains higher than 39% throughout entire frequency range. As shown in Fig. 21(a), the drain efficiencies at 10-dB and 6-dB OBOs are in the range of 39–64% and 40–60%, respectively. It can be seen from Fig. 22 that the gain is maintained around 8–15 dB. Moreover, the PD-ALMBA prototype is measured with a power-swept stimulus at 1-dB step, and the measured efficiency and gain profiles are plotted in Fig. 23. A Doherty-like behavior could be clearly observed from the shape of the efficiency versus output power curves at almost every single

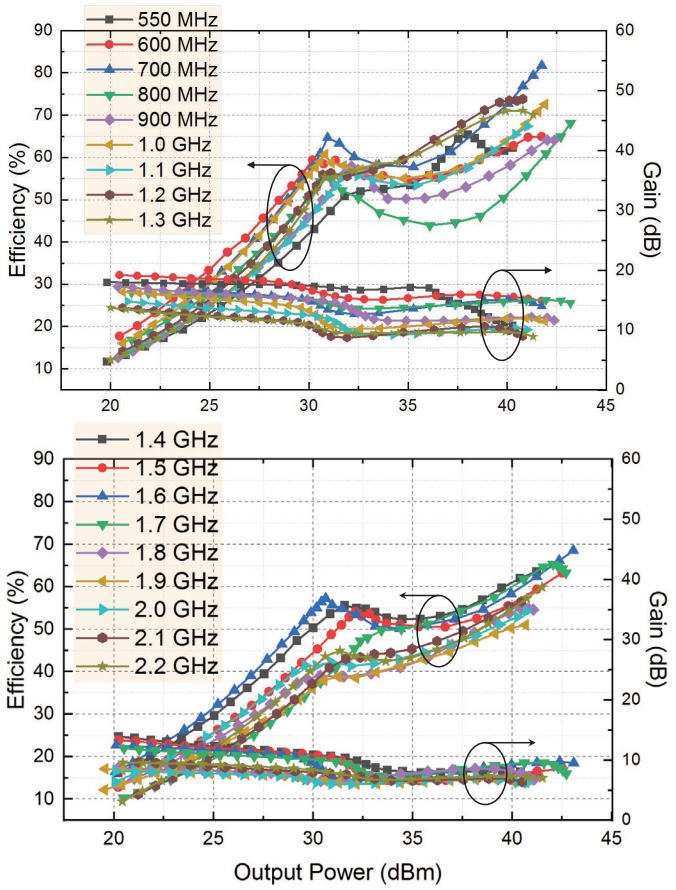

Fig. 23. Power-swept measurement of efficiency and gain from 0.55 to 2.2 GHz.

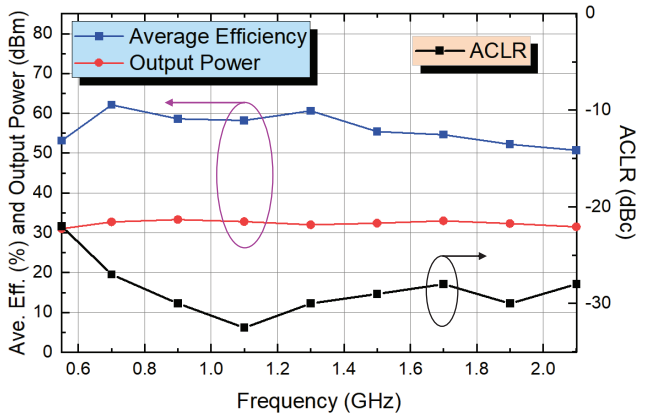

Fig. 24. Measured average drain efficiency, output power, and ACLR with 20-MHz 10.5-dB-PAPR LTE signal at 0.55, 0.7, 0.9, 1.1, 1.3, 1.5, 1.7, 1.9, and 2.1 GHz.

sample frequency point from 0.55–2.2 GHz, while the efficiency is effectively boosted down to 10-dB back-off power, as shown in Fig. 23. These measurement results validate the proposed PD-ALMBA concept and demonstrate the advantage of this new technology in PA efficiency enhancement over ultrawide bandwidth.

Table I presents a comparison between this design and other recently published active-load-modulation PAs with

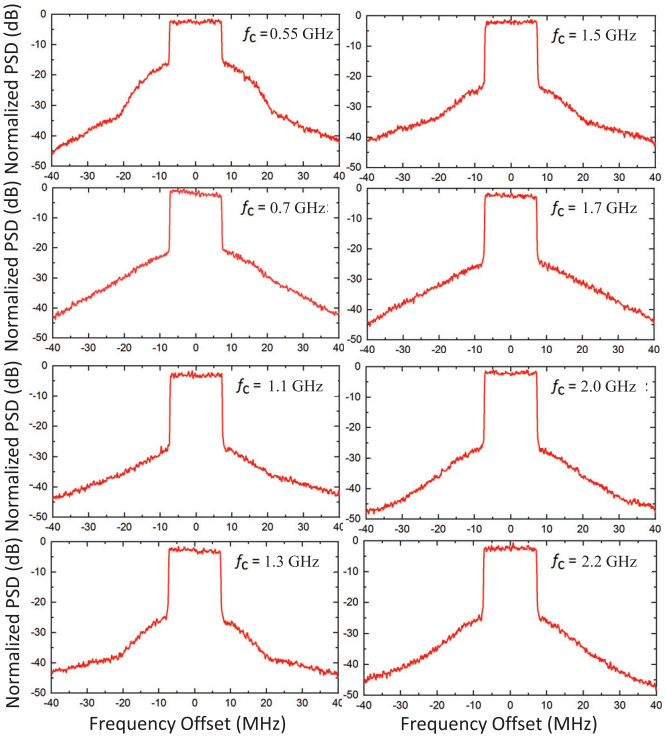

Fig. 25. Output spectrum from modulated measurement using a 20-MHz 10.5-dB-PAPR LTE signal centered at 0.55, 0.7, 1.1, 1.3, 1.5, 1.7, 2.0, and 2.2 GHz.

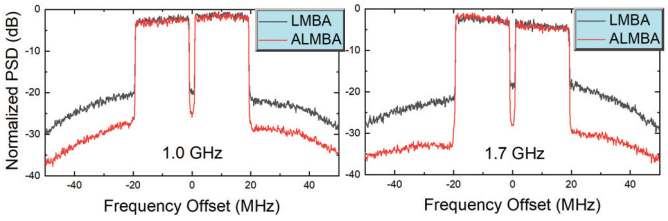

Fig. 26. Output spectrum comparison between PD-LMBA and ALMBA from modulated measurement using a 40-MHz 10.5-dB-PAPR dual-carrier LTE-A signal centered at 1.0 and 1.7 GHz.

similar frequency range, output power level, and technology. As a single-input LMBA architecture, this work significantly advances the state-of-the-art by demonstrating the widest RF bandwidth of two octaves together with efficient PA performance across extended OBO range of $\geq$10 dB.

B. Modulated Measurement

To evaluate the capability of the proposed PD-ALMBA under modulated signal stimulation in realistic communications, a 20-MHz LTE signal with a PAPR of 10 dB is employed as the input. The modulated signal is generated and analyzed by a Keysight PXIe vector transceiver (VXT M9421). The generated LTE signal is further boosted by a linear preamplifier (ZHL-5W-422+) to a sufficient level for driving the developed prototype. The measurement results at an average output power around 33 dBm are presented in Fig. 24. The PD-ALMBA achieves a high average efficiency of 51%–62% over the target frequency

TABLE I
STATE-OF-THE-ART OF WIDEBAND LOAD-MODULATED PAS

Ref. / Year	Architecture	Freq. (GHz)	FBW (%)	P_{Max} (dBm)	DE @ P_{Max} (%)	DE @ HBO (%)	DE @ LBO (%)
[18] 2018	3-Way DPA	0.6-0.9	40	46.1-46.9	51.1-78	51.9-66.2@6 dB	42-64@9.5 dB*
[39] 2018	3-Way DPA	2.0-2.6	26	43.6-45.4	53-76	45-55@6 dB	41-48@8 dB
[40] 2019	3-Way DPA	1.6-2.6	48	45.5-46	53-66	52-66@6 dB	50-53@9.5 dB
[19] 2016	DPA	1.6-2.2	31.6	46-47	60-71	50-55@6 dB*	51-55@10 dB
[41] 2018	DPA	1.5-3.8	86.8	42.3-43.4	42-63	33-55@6 dB	22-40@10 dB*
[17] 2019	DEPA	2.55-3.8	40	48.8-49.8	54-67	42-53@6 dB*	47-60@8 dB
[42] 2017	Dual-Input LMBA	4.5-7.5	50	39	47-77*	28-60@6 dB*	40-72@10 dB*‡
[43] 2018	Dual-Input LMBA	1.7-2.5	38	48-48.9	48-58*	43-53@6 dB*	33-45@10 dB*†
[22] 2017	RF-Input LMBA	0.7-0.85	19	42	57-70	34-48@6 dB	30-35@10 dB*†
[27] 2017	RF-Input LMBA	1.8-3.8	71	44	46-70	33-59@6 dB	20-25@10 dB*†
[20] 2020	Dual-Mode DPA *¶	1.52-4.68	102	41.5	54-71	42-57@6 dB	37-50@10 dB*†
[29] 2020	PD-LMBA	1.5-2.7	57	43	58-72	47-61@6 dB	47-58@10 dB
This Work	PD-ALMBA	0.55-2.2	120	41-43	49-82	40-60@6 dB	39-64@10 dB

* Graphically estimated, † PAE, ‡ with reduced V_{DD}, *¶ with reciprocal gate bias.

band. The measured output power spectral density (PSD) is shown in Fig. 25. The ACLR of most measured frequencies are higher than 28 dB without any digital predistortion. This linearity performance is considerably improved across the entire band in comparison with the ACLR results of PD-LMBA in [29]. In the actual measurement, the drain and gate bias voltages of BA1 and BA2 can be adjusted separately to further optimize the PD-ALMBA linearity. Fig. 26 shows the comparison of the modulated measurement between PD-LMBA (same prototype with symmetrical bias for BA1 and BA2) and PD-ALMBA (asymmetrical bias) using a dual-carrier LTE-Advanced (LTE-A) signal with 40-MHz bandwidth and 10.5-dB PAPR. The linearity is substantially enhanced with up to 10-dB reduction of ACLR at two sample frequencies at 1 and 1.7 GHz, respectively. Overall, the linearity enhancement of PD-ALMBA as compared to PD-LMBA mainly attributes to the reduced CA over-driving and the cooperation with asymmetrical BA1 and BA2.

VI. CONCLUSION

A new load-modulation platform of ALMBA is presented in this article together with the design methodology and implementation. A unified theory of quadrature-coupler based LM PA is unveiled through rigorous analysis and derivation. This new ALMBA theory significantly expands the design space and implementation horizon of conventional LMBA. It is for the first time proved that the CA can be designed with arbitrary LM ratio by properly setting the asymmetry of BA's two sub-amplifiers, BA1 and BA2. Based on Doherty-like biasing of the asymmetric BA1 and BA2 (peaking) and the CA (carrier) with appropriate amplitude and phase controls, the optimal LM performances of three amplifiers can be achieved independently overextended power back-off range and ultrawide RF bandwidth. Moreover, the LM of CA can effectively alleviate the over-driving issue imposed on the symmetric PD-LMBA, thus improving the overall reliability and linearity. The proposed theory and design methodology have been experimentally validated through hardware prototyping, demonstrating the capability of efficiently amplifying a signal with 10-dB PAPR over a 120% fractional bandwidth, which inherits the wideband and high-efficiency characteristics of symmetrical PD-LMBA. This design has significantly advanced the state-of-the-art. Meanwhile, the reduced CA over-driving leads to about 10-dB ACLR reduction over entire bandwidth, which greatly improves the PD-ALMBA linearity and reliability. This proposed PD-ALMBA provides a promising solution for next-generation multiband wireless transmitters.

REFERENCES

[1] R. Wu, Y.-T. Liu, J. Lopez, C. Schecht, Y. Li, and D. Y. C. Lie, "High-efficiency silicon-based envelope-tracking power amplifier design with envelope shaping for broadband wireless applications," *IEEE J. Solid-State Circuits*, vol. 48, no. 9, pp. 2030–2040, Sep. 2013.

[2] A. K. Kwan, M. Younes, O. Hammi, M. Helaoui, and F. M. Ghannouchi, "Linearization of a highly nonlinear envelope tracking power amplifier targeting maximum efficiency," *IEEE Microw. Wireless Compon. Lett.*, vol. 27, no. 1, pp. 82–84, Jan. 2017.

[3] W. H. Doherty, "A new high efficiency power amplifier for modulated waves," *Proc. IRE*, vol. 24, no. 9, pp. 1163–1182, Sep. 1936.

[4] R. Darraji, D. Bhaskar, T. Sharma, M. Helaoui, P. Mousavi, and F. M. Ghannouchi, "Generalized theory and design methodology of wideband Doherty amplifiers applied to the realization of an octave-bandwidth prototype," *IEEE Trans. Microw. Theory Techn.*, vol. 65, no. 8, pp. 3014–3023, Aug. 2017.

[5] V. Camarchia, M. Pirola, R. Quaglia, S. Jee, Y. Cho, and B. Kim, "The Doherty power amplifier: Review of recent solutions and trends," *IEEE Trans. Microw. Theory Techn.*, vol. 63, no. 2, pp. 559–571, Feb. 2015.

[6] A. Banerjee, L. Ding, and R. Hezar, "High efficiency multi-mode outphasing RF power amplifier in 45 nm CMOS," in *Proc. Conf. 41st Eur. Solid-State Circuits Conf. (ESSCIRC)*, Sep. 2015, pp. 168–171.

[7] J. Hur *et al.*, "A multilevel class-D CMOS power amplifier for an outphasing transmitter with a nonisolated power combiner," *IEEE Trans. Circuits Syst. II, Exp. Briefs*, vol. 63, no. 7, pp. 618–622, Jul. 2016.

[8] R. A. Beltran, "Broadband outphasing transmitter using class-E power amplifiers," in *IEEE MTT-S Int. Microw. Symp. Dig.*, Jun. 2019, pp. 67–70.

[9] S. Chung, P. A. Godoy, T. W. Barton, D. J. Perreault, and J. L. Dawson, "Asymmetric multilevel outphasing transmitter using class-E PAs with discrete pulse width modulation," in *IEEE MTT-S Int. Microw. Symp. Dig.*, May 2010, pp. 264–267.

[10] K. Chen and D. Peroulis, "Design of adaptive highly efficient GaN power amplifier for octave-bandwidth application and dynamic load modulation," *IEEE Trans. Microw. Theory Techn.*, vol. 60, no. 6, pp. 1829–1839, Jun. 2012.

[11] C. Sanchez-Perez, M. Ozen, C. M. Andersson, D. Kuylenstierna, N. Rorsman, and C. Fager, "Optimized design of a dual-band power amplifier with SiC varactor-based dynamic load modulation," *IEEE Trans. Microw. Theory Techn.*, vol. 63, no. 8, pp. 2579–2588, Aug. 2015.

[12] H. M. Nemati, C. Fager, U. Gustavsson, R. Jos, and H. Zirath, "Design of varactor-based tunable matching networks for dynamic load modulation of high power amplifiers," *IEEE Trans. Microw. Theory Techn.*, vol. 57, no. 5, pp. 1110–1118, May 2009.
[13] H. M. Nemati, H. Cao, B. Almgren, T. Eriksson, and C. Fager, "Design of highly efficient load modulation transmitter for wideband cellular applications," *IEEE Trans. Microw. Theory Techn.*, vol. 58, no. 11, pp. 2820–2828, Nov. 2010.
[14] C. M. Andersson *et al.*, "Theory and design of class-J power amplifiers with dynamic load modulation," *IEEE Trans. Microw. Theory Techn.*, vol. 60, no. 12, pp. 3778–3786, Dec. 2012.
[15] M. Ozen, K. Andersson, and C. Fager, "Symmetrical Doherty power amplifier with extended efficiency range," *IEEE Trans. Microw. Theory Techn.*, vol. 64, no. 4, pp. 1273–1284, Apr. 2016.
[16] P. Saad, R. Hou, R. Hellberg, and B. Berglund, "An 80 W power amplifier with 50% efficiency at 8 dB power back-off over 2.6–3.8 GHz," in *IEEE MTT-S Int. Microw. Symp. Dig.*, Jun. 2019, pp. 1328–1330.
[17] P. Saad, R. Hou, R. Hellberg, and B. Berglund, "The continuum of load modulation ratio from Doherty to traveling-wave amplifiers," *IEEE Trans. Microw. Theory Techn.*, vol. 67, no. 12, pp. 5101–5113, Dec. 2019.
[18] A. Barthwal, K. Rawat, and S. K. Koul, "A design strategy for bandwidth enhancement in three-stage Doherty power amplifier with extended dynamic range," *IEEE Trans. Microw. Theory Techn.*, vol. 66, no. 2, pp. 1024–1033, Feb. 2018.
[19] J. Xia, M. Yang, and A. Zhu, "Improved Doherty amplifier design with minimum phase delay in output matching network for wideband application," *IEEE Microw. Wireless Compon. Lett.*, vol. 26, no. 11, pp. 915–917, Nov. 2016.
[20] J. Pang, Z. Dai, Y. Li, M. Li, and A. Zhu, "Multiband dual-mode Doherty power amplifier employing phase periodic matching network and reciprocal gate bias for 5G applications," *IEEE Trans. Microw. Theory Techn.*, vol. 68, no. 6, pp. 2382–2397, Jun. 2020.
[21] D. J. Shepphard, J. Powell, and S. C. Cripps, "An efficient broadband reconfigurable power amplifier using active load modulation," *IEEE Microw. Wireless Compon. Lett.*, vol. 26, no. 6, pp. 443–445, Jun. 2016.
[22] P. H. Pednekar and T. W. Barton, "RF-input load modulated balanced amplifier," in *IEEE MTT-S Int. Microw. Symp. Dig.*, Jun. 2017, pp. 1730–1733.
[23] D. Collins, R. Quaglia, J. Powell, and S. Cripps, "Experimental characterization of a load modulated balanced amplifier with simplified input power splitter," in *Proc. Asia–Pacific Microw. Conf. (APMC)*, Nov. 2018, pp. 461–463.
[24] T. Cappello, P. Pednekar, C. Florian, S. Cripps, Z. Popovic, and T. W. Barton, "Supply- and load-modulated balanced amplifier for efficient broadband 5G base stations," *IEEE Trans. Microw. Theory Techn.*, vol. 67, no. 7, pp. 3122–3133, Jul. 2019.
[25] H. Jeon *et al.*, "A triple-mode balanced linear CMOS power amplifier using a switched-quadrature coupler," *IEEE J. Solid-State Circuits*, vol. 47, no. 9, pp. 2019–2032, Sep. 2012.
[26] T. Cappello, P. H. Pednekar, C. Florian, Z. Popovic, and T. W. Barton, "Supply modulation of a broadband load modulated balanced amplifier," in *IEEE MTT-S Int. Microw. Symp. Dig.*, Jun. 2018, pp. 304–307.
[27] P. H. Pednekar, E. Berry, and T. W. Barton, "RF-input load modulated balanced amplifier with octave bandwidth," *IEEE Trans. Microw. Theory Techn.*, vol. 65, no. 12, pp. 5181–5191, Dec. 2017.
[28] Y. Cao, H. Lyu, and K. Chen, "Load modulated balanced amplifier with reconfigurable phase control for extended dynamic range," in *IEEE MTT-S Int. Microw. Symp. Dig.*, Jun. 2019, pp. 1335–1338.
[29] Y. Cao and K. Chen, "Pseudo-Doherty load-modulated balanced amplifier with wide bandwidth and extended power back-off range," *IEEE Trans. Microw. Theory Techn.*, vol. 68, no. 7, pp. 3172–3183, Jul. 2020.
[30] J. Pang *et al.*, "Analysis and design of highly efficient wideband RF-input sequential load modulated balanced power amplifier," *IEEE Trans. Microw. Theory Techn.*, vol. 68, no. 5, pp. 1741–1753, May 2020.
[31] P. Saad, R. Hou, R. Hellberg, and B. Berglund, "Ultrawideband Doherty-like power amplifier," in *IEEE MTT-S Int. Microw. Symp. Dig.*, Jun. 2018, pp. 1215–1218.
[32] P. Saad, R. Hou, R. Hellberg, and B. Berglund, "A 1.8–3.8-GHz power amplifier with 40% efficiency at 8-dB power back-off," *IEEE Trans. Microw. Theory Techn.*, vol. 66, no. 11, pp. 4870–4882, Nov. 2018.
[33] H. Lyu and K. Chen, "Balanced-to-Doherty mode-reconfigurable power amplifier with high efficiency and linearity against load mismatch," *IEEE Trans. Microw. Theory Techn.*, vol. 68, no. 5, pp. 1717–1728, May 2020.
[34] S. C. Cripps, *RF Power Amplifiers for Wireless Communications*, 2nd ed. Norwood, MA, USA: Artech House, 2006, pp. 323–326.
[35] Y. Cao and K. Chen, "Dual-octave-bandwidth RF-input pseudo-Doherty load modulated balanced amplifier with $\geq$ 10-dB power back-off range," in *IEEE MTT-S Int. Microw. Symp. Dig.*, 2020, Paper IMS2020.
[36] K. Chen and D. Peroulis, "Design of highly efficient broadband class-E power amplifier using synthesized low-pass matching networks," *IEEE Trans. Microw. Theory Techn.*, vol. 59, no. 12, pp. 3162–3173, Dec. 2011.
[37] K. Chen and D. Peroulis, "Design of broadband highly efficient harmonic-tuned power amplifier using in-band continuous class-F^{-1}/F mode transferring," *IEEE Trans. Microw. Theory Techn.*, vol. 60, no. 12, pp. 4107–4116, Dec. 2012.
[38] P. Saad, C. Fager, H. Cao, H. Zirath, and K. Andersson, "Design of a highly efficient 2–4-GHz octave bandwidth GaN-HEMT power amplifier," *IEEE Trans. Microw. Theory Techn.*, vol. 58, pp. 1677–1685, Jul. 2010.
[39] S. Chen, W. Wang, K. Xu, and G. Wang, "A reactance compensated three-device Doherty power amplifier for bandwidth and back-off range extension," *Wireless Commun. Mobile Comput.*, vol. 2018, pp. 1–10, Jan. 2018, doi: 10.1155/2018/8418165.
[40] J. Xia, W. Chen, F. Meng, C. Yu, and X. Zhu, "Improved three-stage Doherty amplifier design with impedance compensation in load combiner for broadband applications," *IEEE Trans. Microw. Theory Techn.*, vol. 67, no. 2, pp. 778–786, Feb. 2019.
[41] J. J. M. Rubio, V. Camarchia, M. Pirola, and R. Quaglia, "Design of an 87% fractional bandwidth Doherty power amplifier supported by a simplified bandwidth estimation method," *IEEE Trans. Microw. Theory Techn.*, vol. 66, no. 3, pp. 1319–1327, Mar. 2018.
[42] D. J. Shepphard, J. Powell, and S. C. Cripps, "A broadband reconfigurable load modulated balanced amplifier (LMBA)," in *IEEE MTT-S Int. Microw. Symp. Dig.*, Jun. 2017, pp. 947–949.
[43] R. Quaglia and S. Cripps, "A load modulated balanced amplifier for telecom applications," *IEEE Trans. Microw. Theory Techn.*, vol. 66, no. 3, pp. 1328–1338, Mar. 2018.

Yuchen Cao (Graduate Student Member, IEEE) received the bachelor's degree in engineering from Zhejiang University, Hangzhou, Zhejiang, China, in 2011, and the master's degree from Wichita State University, Wichita, KS, USA, in 2016. He is currently pursuing the Ph.D. degree at the Electrical and Computer Engineering Department, University of Central Florida, Orlando, FL, USA.

His research interests include highly efficient broadband PAs, carrier aggregation, and millimeter-wave circuit design.

Mr. Cao was a recipient of the First Place Award of the Student Paper Competition in the IEEE Microwave Theory and Techniques Society (IEEE MTT-S) International Microwave Symposium (IMS) 2020, the First Place Award of the Student Design Competition on "Carrier Aggregation BAW Quadplexer Module" in IEEE MTT-S IMS, in 2018 and 2019, respectively, the Second Place Award of Student Paper Competition in IEEE WAMICON 2019, and the Third Place Award of the Student Design Competition on "High Efficiency Power Amplifier" in IEEE MTT-S IMS 2019.

Haifeng Lyu (Graduate Student Member, IEEE) received the bachelor's degree in electrical engineering and automation from the Chengdu University of Technology, Chengdu, Sichuan, China, in 2010, and the master's degree in electrical engineering from the University of Rhode Island, Kingston, RI, USA, in 2017. He is currently pursuing the Ph.D. degree at the University of Central Florida, Orlando, FL, USA.

His research interests include novel highly efficient and linear power amplifier (PA) architectures and reconfigurable RF/mm-wave circuits.

Mr. Lyu was the winner of Student Design Competitions, including High Efficiency Power Amplifier and Carrier Aggregation BAW Quadplexer Module in IEEE MTT-S International Microwave Symposium (IMS) 2019.

Kenle Chen (Member, IEEE) received the bachelor's degree in communication engineering from Xi'an Jiaotong University, Xi'an, Shaanxi, China, in 2005, the master's degree in electronics and information engineering from Peking University, Beijing, China, in 2008, and the Ph.D. degree in electrical engineering from Purdue University, West Lafayette, IN, USA, in 2013.

He has extensive experiences in wireless and semiconductor industries. From 2015 to 2017, he worked as a Staff RFIC Engineer with Skyworks Solutions, Inc., San Jose, CA, USA, where he focused on development of RF frontend modules for advanced mobile platforms. From 2013 to 2015, he worked as a Principal/Lead RFIC Engineer with innovational startups, where he led the Research & Development of multiple successful products of CMOS integrated power amplifiers and frontend solutions for the latest WLAN platforms, e.g., IEEE802.11ac/ax. He is currently an Assistant Professor with the Department of Electrical and Computer Engineering, University of Central Florida, Orlando, FL, USA. His research interests include energy-efficient, wideband, and ultrahigh-speed RF/mm-Wave circuits, extreme-performance power amplifiers in CMOS and compound semiconductor technologies, reconfigurable RF/mm-Wave electronics, and innovational wireless radio architectures & applications.

Dr. Chen is an Associate Editor of the IEEE TRANSACTIONS ON MICROWAVE THEORY AND TECHNIQUES. He serves as the Chair for the IEEE MTT-S/AP-S Orlando Chapter.